

RESEARCH ARTICLE

A distinct epigenetic profile distinguishes stenotic from non-inflamed fibroblasts in the ileal mucosa of Crohn's disease patients

Andrew Y. F. Li Yim^{1,2}, Jessica R. de Bruyn^{3,4}, Nicolette W. Duijvis³, Catriona Sharp², Enrico Ferrero⁶, Wouter J. de Jonge³, Manon E. Wildenberg³, Marcel M. A. M. Mannens¹, Christianne J. Buskens⁵, Geert R. D'Haens⁴, Peter Henneman¹, Anje A. te Velde³*

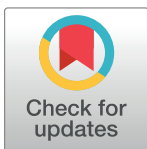
1 Genome Diagnostics Laboratory, Department of Clinical Genetics, Amsterdam UMC, University of Amsterdam, Amsterdam, the Netherlands, **2** Epigenetics Discovery Performance Unit, GlaxoSmithKline, Stevenage, United Kingdom, **3** Tytgat Institute for Liver and Intestinal Research, Amsterdam UMC, University of Amsterdam, Amsterdam, the Netherlands, **4** Department of Gastroenterology, Amsterdam UMC, University of Amsterdam, Amsterdam, the Netherlands, **5** Department of Surgery, Amsterdam UMC, University of Amsterdam, Amsterdam, the Netherlands, **6** Computational Biology, Target Sciences, GlaxoSmithKline, Stevenage, United Kingdom

☯ These authors contributed equally to this work.

✉ Current address: Autoimmunity Transplantation and Inflammation Bioinformatics, Novartis Institutes for Biomedical Research, Basel, Switzerland.

‡ These authors are joint senior authors on this work.

* a.a.tevelde@amc.nl



OPEN ACCESS

Citation: Li Yim AYF, de Bruyn JR, Duijvis NW, Sharp C, Ferrero E, de Jonge WJ, et al. (2018) A distinct epigenetic profile distinguishes stenotic from non-inflamed fibroblasts in the ileal mucosa of Crohn's disease patients. PLoS ONE 13(12): e0209656. <https://doi.org/10.1371/journal.pone.0209656>

Editor: Osman El-Maarri, University of Bonn, Institute of Experimental Hematology and Transfusion Medicine, GERMANY

Received: May 11, 2018

Accepted: December 10, 2018

Published: December 27, 2018

Copyright: © 2018 Li Yim et al. This is an open access article distributed under the terms of the [Creative Commons Attribution License](https://creativecommons.org/licenses/by/4.0/), which permits unrestricted use, distribution, and reproduction in any medium, provided the original author and source are credited.

Data Availability Statement: Both the raw and the processed data have been made publicly available in the GEO database (accession numbers: GSE99788 and GSE99816 for the DNA methylation and RNA sequencing experiments, respectively). The scripts used for data analysis are located at https://github.com/ND91/PRJ000003_LiYim2018.

Abstract

Background

The chronic remitting and relapsing intestinal inflammation characteristic of Crohn's disease frequently leads to fibrosis and subsequent stenosis of the inflamed region. Approximately a third of all Crohn's disease patients require resection at some stage in their disease course. As the pathogenesis of Crohn's disease associated fibrosis is largely unknown, a strong necessity exists to better understand the pathophysiology thereof.

Methods

In this study, we investigated changes of the DNA methylome and transcriptome of ileum-derived fibroblasts associated to the occurrence of Crohn's disease associated fibrosis. Eighteen samples were included in a DNA methylation array and twenty-one samples were used for RNA sequencing.

Results

Most differentially methylated regions and differentially expressed genes were observed when comparing stenotic with non-inflamed samples. By contrast, few differences were observed when comparing Crohn's disease with non-Crohn's disease, or inflamed with non-inflamed tissue. Integrative methylation and gene expression analyses revealed dysregulation of genes

Funding: This work was supported by the European Commission, Horizon 2020 Framework Programme (SEP-210163258 to WJJ) and the European Crohn's and Colitis Organisation (project: 'DNA methylation profiles in IBD fibroblasts' to AAV and PH). WJJ was a co-owner of Gut Research BV at the time of writing this manuscript. GlaxoSmithKline provided support in the form of salaries for authors AYFLY and CS and GlaxoSmithKline and Novartis provided support in the form of salaries for author EF. GlaxoSmithKline, Novartis and Gut Research BV had no additional role in the study design, data collection and analysis, decision to publish, or preparation of the manuscript. The specific roles of these authors are articulated in the 'author contributions' section.

Competing interests: We have the following interests: GlaxoSmithKline provided support in the form of salaries for authors AYFLY and CS and GlaxoSmithKline and Novartis provided support in the form of salaries for author EF. WJJ was financially supported by GlaxoSmithKline, Maed Johansson, Schwabe (aforementioned funds were unrelated to this study) and was a co-owner of Gut Research BV at the time of writing this manuscript. There are no patents, products in development or marketed products to declare. This does not alter our adherence to all the PLOS ONE policies on sharing data and materials.

Abbreviations: CD, Crohn's disease; IBD, Inflammatory bowel disease; GWAS, Genome-wide association study; EWAS, Epigenome-wide association study; ECM, Extracellular matrix; NINF, CD Non-inflamed tissue; INF, CD Inflamed tissue; STEN, CD Stenotic tissue; CpG, Cytosine followed by a guanine; DMP, Differentially methylated position; DMR, Differentially methylated region; DEG, Differentially expressed gene; DMEG, Differentially methylated and expressed gene; eQTM, Expression quantitative trait methylation; TSS, Transcription start site.

associated to the PRKACA and E2F1 network, which is involved in cell cycle progression, angiogenesis, epithelial to mesenchymal transition, and bile metabolism.

Conclusion

Our research provides evidence that the methylome and the transcriptome are systematically dysregulated in stenosis-associated fibroblasts.

Introduction

Crohn's disease (CD) is a chronic condition characterized by repeated episodes of transmural inflammation in the gastrointestinal tract. While most patients display a purely inflammatory phenotype during diagnosis, fibro-stenotic complications occur in approximately a third of patients as the disease progresses. Stenosis, as a result of fibrotic tissue accumulation, is a serious complication for which no current predictors or therapeutic treatments exist, often requiring the surgical removal of the afflicted region [1]. As such, there is a strong necessity to understand the pathophysiology of CD-induced fibrosis, to allow for the development diagnostic markers and treatments.

Fibrosis is characterized by the expansion of the resident fibroblast population as well as the result of excessive production and deposition of extracellular matrix (ECM), which leads to local tissue stiffness and ultimately stenosis of the intestinal lumen [2,3]. The cause of CD-associated fibrosis is thought to be persistent tissue injury, which in turn results in the dysregulation of wound healing, unrestrained proliferation of fibroblasts, and accumulation of ECM [4]. The aberrant wound healing process, in combination with the accumulation of ECM, eventually leads to fibrosis, which may become self-propagating [5].

Genome-wide association studies (GWAS) have identified over 200 loci associated to inflammatory bowel disease (IBD) [6], many of which either associate to several genes or are not annotated. Despite the extensive research into the genetic component underlying IBD, it is estimated that common genetic variants explain only 20% of the estimated heritability (30–50%) [6–8]. Therefore, IBD has been classified as a complex disease, the etiology of which is likely a combination of genetic [9], epigenetic [10–13] and other environmental factors [7,14].

Epigenetic modifications affect the readability and transcription of the genome without changing the actual sequence. The dynamic behavior of the epigenetic landscape is partially a response to environmental influences, suggesting a putative link between CD-associated fibrosis and the environment [15,16]. One of the most widely investigated epigenetic modifications is cytosine methylation, with previous epigenome-wide association studies (EWAS) investigating CD and IBD in leukocytes reporting many differentially methylated loci in genes that are part of inflammatory and immune related pathways [17–22]. Despite the many statistically significant loci, the actual differences in methylation were often small (<20% mean methylation difference). In contrast, samples derived from the ileocolon revealed larger changes in DNA methylation [23,24], suggesting that the methylome is more profoundly affected at the sites of inflammation rather than in peripheral tissues. Here, we investigated whether fibro-stenosis manifests itself within the DNA methylome and transcriptome to identify putative drivers of the fibro-stenotic phenotype by comparing CD and non-CD, as well as among different stages of CD. In particular, we chose to investigate ileal fibroblasts, as fibro-stenosis with complications occur primarily in the terminal ileum of CD patients [25].

Materials and methods

Patient and sample selection

Fibroblasts were isolated from the mucosa of terminal ileal tissue of CD patients undergoing ileocecal resection surgery due to therapy-refractory disease at the Academic Medical Center in Amsterdam, the Netherlands (Table 1). The CD fibroblasts were isolated from the mucosa of the ileum, which appeared macroscopically normal ('non-inflamed'; NINF), inflamed (INF), or stenotic (STEN), as determined by the treating surgeon and confirmed by qualified researchers in the laboratory. The control fibroblasts were obtained from patients without a history of IBD who underwent resection for colon ascendance malignancies. Fibroblasts were isolated from mucosal tissue at a distance of at least 10 cm from neoplastic lesions to minimize tumor involvement [26]. In addition to the phenotypic appearance of the sample of origin, additional metadata such as age, sex, current treatment, smoking status, and Montreal classification [27] were documented as well (Table 1).

An overview of all the samples included in the DNA methylation and the RNA sequencing experiments is provided in S1 Table. In short, the DNA methylation experiment was performed on 18 samples isolated from 10 unique patients (7 NINF from 4 patients, 2 INF from 2 patients, 4 STEN from 3 patients, and 5 non-CD from 3 control patients). The RNA sequencing experiment was performed on 21 samples isolated from 14 unique patients (6 NINF from 6 patients, 4 INF from 4 patients, 5 STEN from 4 patients, and 6 non-CD from the 4 control

Table 1. Patient characteristics.

| A | | | | |
|--|---------------|---------|---------|----------------|
| DNA | CD (n = 7) | | | non-CD (n = 3) |
| Age at time of surgery (mean ± standard deviation) | 29.7 (± 10.3) | | | 46 (± 22.6) |
| Sex (% males; n) | 71% (5) | | | 66% (2) |
| Current treatment with biological agent (% yes; n) | 71% (5) | | | - |
| Current smokers (% yes; n) | 28% (2) | | | 0% (0) |
| Montreal classification (%; n) | | | | - |
| A1 / A2 / A3 | 14% (1) | 86% (6) | 0% | |
| L1 / L2 / L3 / L4 | 57% (4) | 0% | 43% (3) | 0% |
| B1 / B2 / B3 / B2+B3 | 14% (1) | 29% (2) | 14% (1) | 43% (3) |
| P | 29% (2) | | | |
| B | | | | |
| RNA | CD (n = 10) | | | non-CD (n = 4) |
| Age at time of surgery (mean ± standard deviation) | 35.7 (± 14.4) | | | 54.5 (± 18.3) |
| Sex (% males; n) | 60% (6) | | | 75% (3) |
| Current treatment with biological agent (% yes; n) | 60% (6) | | | - |
| Current smokers (% yes; n) | 20% (2) | | | 0% (0) |
| Montreal classification (%; n) | | | | - |
| A1 / A2 / A3 | 10% (1) | 90% (9) | 0% | |
| L1 / L2 / L3 / L4 | 50% (5) | 0% | 50% (5) | 0% |
| B1 / B2 / B3 / B2+3 | 20% (2) | 30% (3) | 20% (2) | 30% (3) |
| P | 10% (1) | | | |

Overview of the samples used in the DNA methylation and gene expression experiments. The Montreal classification represents a scale which is used to classify disease severity of IBD.

<https://doi.org/10.1371/journal.pone.0209656.t001>

patients). Of the samples used for DNA methylation and RNA sequencing, 9 from 6 unique patients were present in both experiments.

Fibroblast isolation

Mucosal samples were thoroughly washed in repeated cycles of ice-cold phosphate buffered saline (PBS) supplemented with 1% penicillin/streptomycin and 40 µg/mL gentamicin (PGA). The mucosa was then finely cut and placed in full-grown RPMI 1640 culture medium (Invitrogen) supplemented with 1.5 mg/mL collagenase A (Roche, Germany) and minced using the GentleMACs Dissociator (Miltenyi Biotec, Leiden, the Netherlands). After 60 minutes of incubation at 37°C, the GentleMACs Dissociator was used a second time for further dissociation. Cells were transferred to tubes and washed extensively with PGA, after which the cells were plated and cultured at 37°C in RPMI 1640 with 10% FCS, 1% penicillin/streptomycin, 1% L-glutamin, 40 µg/mL gentamicin (Lonza, Leusden, the Netherlands) and 0.025 µg/mL amphotericin B (Gibco, Rockford, IL) [28].

Immunohistochemistry

Tissue was fixed in 4% paraformaldehyde, embedded in paraffin and sectioned at 4 micrometer. Sections deparaffinized, rehydrated and immersed in 0.3% H₂O₂ and methanol for 30 minutes. Antigen-retrieval was performed using Tris-EDTA (CD3) or NaCi (collagen type I) after which slides were blocked with PBS, 0.1% Triton X-100 and 1% bovine serum albumin (PBT) for 30 minutes. Slides were subsequently incubated with the primary antibody overnight at 4°C (rabbit monoclonal anti-human CD3 [clone SP7, Thermo Scientific] and goat polyclonal collagen I [Southern Biotech, Birmingham, AL, USA]) in PBT, after which they were incubated with Brightvision [Immunologic, Duiven, the Netherlands], developed using DAP, counterstained with haematoxylin and mounted.

Passaging and harvesting of fibroblasts

After 24 hours of culturing, fibroblast cells were adhered to the culture plates and the RPMI medium was refreshed to wash away debris, dead-, non-adherent- and non-fibroblast cells. After the cells reached a minimum of 80% confluency, they were washed with HBSS (Lonza BioWhittaker, Switzerland) and detached from the culture plates through a ten-minute trypsin wash (10x diluted in HBSS) at 37°C. The fibroblasts were then plated in T25 flasks, after which samples in later passages were transferred to T75 flasks (VWR, Pennsylvania, USA; Tissue Culture Flasks 25 cm² & 75 cm²) to allow for further expansion. During passages 1 through 5, cells were harvested for downstream DNA and RNA analysis. For DNA isolation, fibroblasts were stored in PBS at -80°C, while cells for RNA isolation were stored in RNeasy Lysis Buffer (Qiagen, Crawley, UK) at 4°C overnight, after which the samples were transferred to -80°C as per manufacturer's protocol. Eighteen DNA samples were isolated from 10 unique patients for the methylation experiment, whereas 25 RNA samples were isolated from 15 unique patients for the RNA sequencing experiment.

Methylation analysis

Analysis of the methylation data was performed in the R statistical programming environment [29] (v3.3.2) using the Bioconductor (v3.4) packages minfi [30] (v1.24.0) for import, MethyLAid [31] (v1.12.0) for quality control, functional normalization for normalization [32], limma [33,34] (v3.34.9) for linear regressions to find differentially methylated positions (DMPs), and DMRcate [35] (v1.14.0) to find differentially methylated regions (DMRs). Regions were found

to be differentially methylated if it contained at least 3 CpG-probes. Annotation of the DMRs was performed using ChIPSeeker [36], which associates regions of interest to genes according to their location relative to the nearest transcription start site (TSS). Samples were included in this study if they passed the detection *p*-value quality control and were not an outlier according to the principal component analysis. Probes were excluded from the analyses if their CpG of interest overlapped with a known SNP (minor allele frequency > 0.05), if the probe was found to be promiscuous [37]. Furthermore, all probes associating to the sex chromosomes were removed due to the mixed-sex cohort. Statistical significance was defined as DMRs that had a Stouffer transformed Benjamini-Hochberg (BH) adjusted *p*-value below 0.05. Linear regressions were performed using the M-values, whereas the Beta-values were utilized for the visualization [38]. Covariates in the DMP and DMR analyses included passage number, age, sex, and medication usage (azathioprine, purinethol, adalimumab, or infliximab). An additional random effects component ('blocking') for patient source was utilized to correct for samples obtained from the same patient. Plots were made using ggplot2 (v2.2.1) [39].

Metadata anonymous sample

Due to the anonymity of one control sample, no metadata was available. The age and sex were therefore estimated using the DNA methylation and gene expression data. The age was estimated using 353 age-related CpG sites as described by Horvath [40], after which the age-related CpG sites were removed to prevent any confounding of downstream analyses. The sex was estimated based on the presence of a methylation signal of probes located on chromosome Y and was subsequently confirmed by the presence of gene expression signals coming from chromosome Y.

Gene expression analysis

RNA was isolated from the fibroblasts using the RNAeasy mini kit (Qiagen) and the quality was measured using the BioAnalyzer, whereby RNA samples with a RIN score of 8 or higher were taken for further analysis. The NEBNext Ultra Directional RNA Library Prep Kit (New England BioLabs) was used for mRNA isolation, cDNA generation, and sequencing adapter ligation. Next generation sequencing of the resulting cDNA libraries was performed on an Illumina NextSeq500 at a coverage of 10M reads per sample. The preparation and sequencing of the RNA was performed at GenomeScan B.V. in Leiden, the Netherlands (ISO/IEC 17025 (L518) accredited).

For the differential gene expression analysis, raw sequences were merged per sample and checked for quality using FastQC [41] (v1.11.7) and MultiQC (v1.4). The sequences were then aligned to the reference genome GRCh38 using STAR [42] (v2.5), and sorted and converted into binary files using SAMtools [43] (v1.2). Reads were counted and annotated using the Ensembl annotations (v90) using the featureCounts module in the Subread package [44] (v1.28). Subsequent normalization and differential gene expression analysis was performed using DESeq2 [45] (v1.18.1). Similar to the methylation analysis, we corrected for passage number, age, sex, and medication usage (azathioprine, purinethol, adalimumab, or infliximab). Genes were excluded if the count per million (CPM) had been less than 1 for more than 11 samples. Plots were made using ggplot2 [39].

Integrative methylation-expression analysis

Genes that were differentially expressed and differentially methylated (DMEGs) were extracted and subjected to an expression quantitative trait methylation analysis (eQTM). In short DMRs were correlated with the log transformed count data obtained from the expression analysis for

the 9 samples that were analyzed in both the methylation and the expression analysis (S1 Table). The mean Beta value per DMR was calculated per sample after which Pearson correlations were calculated for each DMR-gene pair. The 95% confidence intervals were calculated through 10000 bootstraps and *p*-values were calculated by comparing our observed correlation coefficient against a permutation-based null-distribution. The null-distribution was generated by randomly generating 10000 regions with equal numbers of CpGs as the observed DMR ('null-DMRs'). Resulting plots were generated using Gviz (v1.22.3) [46] and ggplot2 [39].

Pathway enrichment and gene set overrepresentation analyses

As DMRs, DEGs and DMEGs represent different entities, different tools were used for pathway enrichment and gene set overrepresentation analyses. DMRs represent genomic regions and thus we performed pathway enrichment analyses using the ChIP-Enrich (v2.2.0) package to account for the length of the DMR [47]. Conversely, DESeq2 normalizes for the locus length during differential expression analysis, which does not need to be corrected for during the enrichment analysis. Instead, pathway enrichment analyses of the DEGs were performed using the camera function from limma [48], which performs a competitive gene set test to account for inter-gene correlation. For the enrichment analyses of the DMRs and the DEGs, the Reactome [49] and Kyoto Encyclopedia of Genes and Genomes (KEGG) [50] pathway databases were used as reference datasets. To obtain a summary of the observed DMEGs regardless of the direction of methylation or expression we used the ConsensusPath database webtool, where we performed gene set overrepresentation analyses against the network neighborhood-based entity sets (NESTs), all available pathway gene sets, and the protein complex-based gene sets [51].

Data availability

Both the raw and the processed data have been made publicly available in the GEO repository GSE99788 and GSE99816 for the DNA methylation and RNA sequencing experiments, respectively. The scripts used for data analysis are located at https://github.com/ND91/PRJ0000003_LiYim2018.

Ethical considerations

Part of the patient samples were acquired from the surgical department with signed informed consent prior to surgery, as reviewed and approved by the institutional ethics committee at the Academic Medical Center Amsterdam ("Medisch Ethische Toetsings Commissie AMC", reference: METC #2014_178). Other patient samples were collected from the pathology department and were granted a waiver by the institutional ethics committee (reference: W12_216 # 12.17.0246).

Results

Genome-wide differences in methylation when comparing stenotic with non-inflamed tissue

Ileal material was obtained from CD and non-CD patients undergoing resection after which it was macroscopically classified into non-inflamed (NINF), inflamed (INF), and stenotic (STEN) tissue. Immunohistochemical staining for CD3 showed that INF tissue displayed more CD3+ cells relative to the NINF and the STEN tissue samples. Furthermore, general staining for hematoxylin and eosin (HE) as well as specific staining for collagen indicated that the STEN samples are mainly fibrotic in nature as shown by extensive collagen deposition (Fig 1A). It should be noted that as the STEN samples are obtained from an affected area, levels of

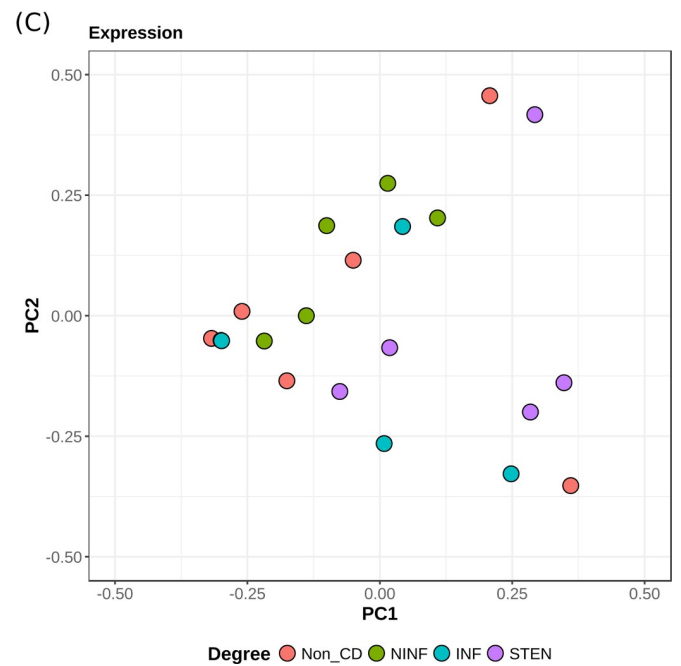
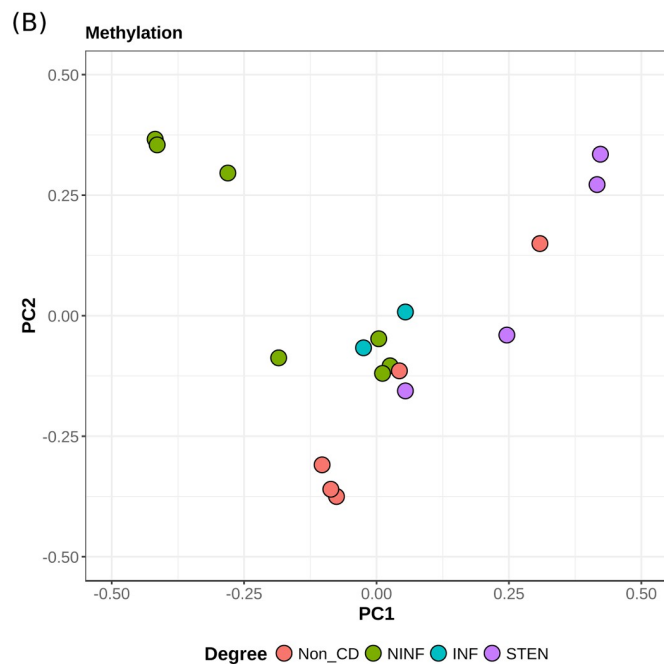
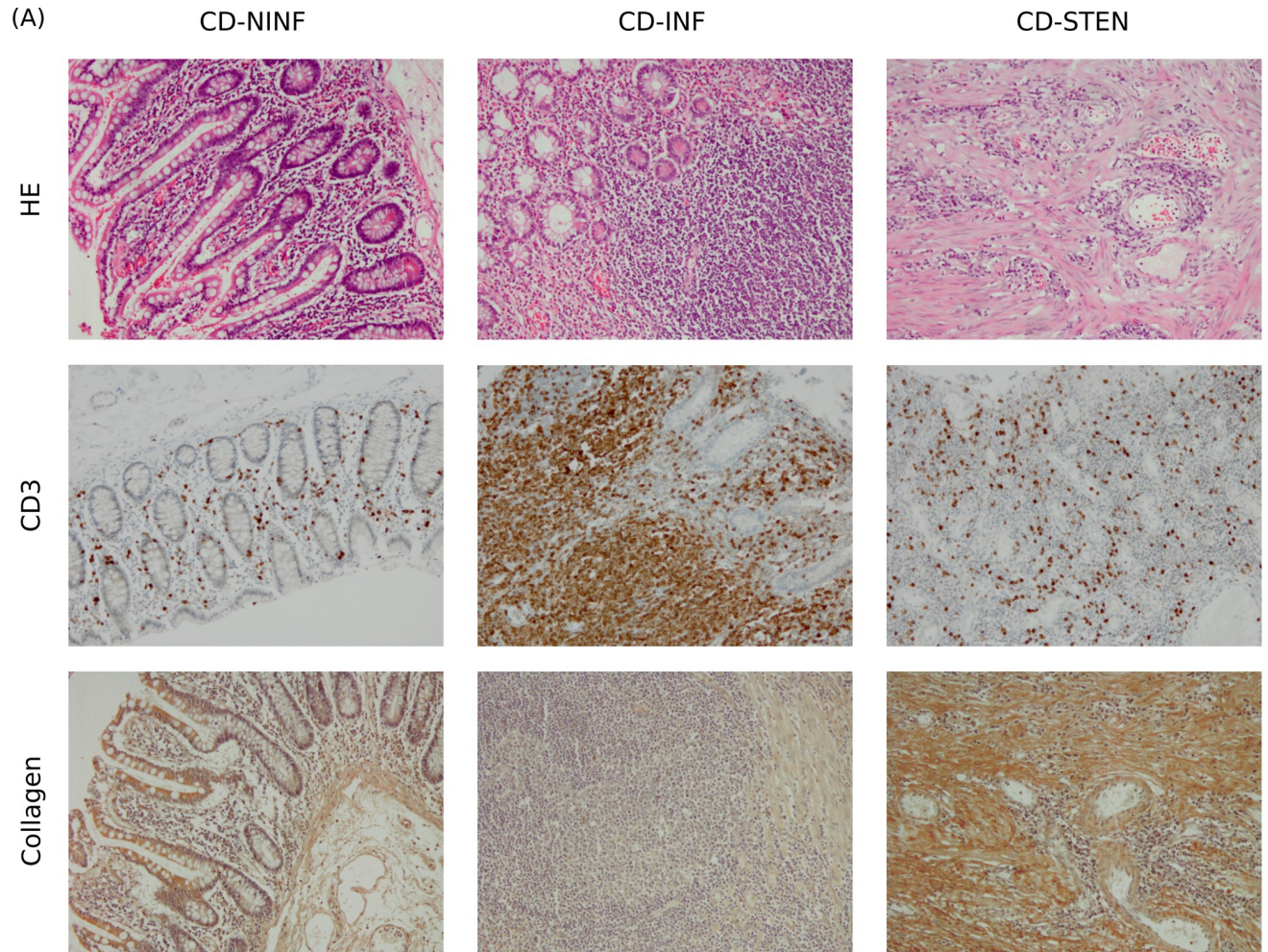


Fig 1. Immunohistochemical staining and principal component analyses. (A) General staining for haematoxylin and eosin (HE) and specific staining for CD3 and collagen. Principal components 1 and 2 for (B) DNA methylation, and (C) gene expression.

<https://doi.org/10.1371/journal.pone.0209656.g001>

CD3 infiltration are increased relative to NINF samples, albeit far below the levels seen in the INF samples (Fig 1A). Mucosal fibroblasts were subsequently extracted from the resection material and cultured to prevent the growth of other cell types.

We were primarily interested in differences in methylation and expression between (i) CD and non-CD patients, as well as the comparisons within CD patients: (ii) INF vs NINF and (iii) STEN vs NINF. As the fibroblasts had been cultured and grown to different passages, we investigated whether any effect was evident at a genome-wide level by means of principal component analysis (PCA). We observed limited to no correlation between passage and the first three principal components for both the methylation and the expression data ($r^2_{\text{passage}} < 0.3$), suggesting that passage does not affect the methylation or gene expression overall (S1 Fig). In addition, we correlated the principal components with the other factors: CD degree, age, sex, smoker status and medication usage. Limited correlation was observed between medication usage and the first three principal components ($r^2_{\text{medication}} < 0.2$). Sex and age however were moderately correlated with the second principal component for the methylation data ($r^2_{\text{sex}} = 0.41$; $r^2_{\text{age}} = 0.53$) and the moderately with the first principal component for the expression data ($r^2_{\text{sex}} = -0.05$; $r^2_{\text{age}} = 0.26$). Interestingly, the strongest correlation with the first principal component for the methylation data was observed for NINF < INF < STEN ($r^2_{\text{degree CD}} = 0.46$). Visualization of the first two principal components for the methylation data revealed a clear distinction between STEN and NINF tissue (Fig 1B), suggesting genome-wide differences in methylation. However, visualization of the first two principal components of the gene expression data did not show any separation among the different degrees of CD (Fig 1C). To mitigate the effect of the passage, sex, age and medication usage, they were included as covariates in the downstream linear regression analyses.

Stenosis-associated differentially methylated regions affect tissue remodeling processes

Systematically searching for differentially methylated positions (DMPs) yielded 44, 84621, and 123877 DMPs when comparing CD with non-CD, CD INF with CD NINF and CD STEN with CD NINF, respectively (Table 2). In agreement with the PCA, most DMPs were found when comparing STEN with NINF fibroblasts (S2 Fig). We reasoned that continuous regions of differential methylation (DMRs) are more likely biologically relevant and therefore investigated the presence of DMRs. In total, 38, 4, and 4883 DMRs were found for the comparisons CD with non-CD, INF with NINF, and STEN with NINF, respectively (Tables 2 and S2). For the CD with non-CD and the STEN with NINF comparisons we observed several genes to be affected by multiple DMRs. By summing the lengths of the DMRs per gene and then sorting them, we observed long regions (>3 kbps) of differential methylation for Wnt family member

Table 2. Results overview.

| Comparison | DMPs | DMRs | DEGs |
|--------------------|---------|-------|------|
| CD vs Non-CD | 44 | 38 | 11 |
| CD-INF vs CD-NINF | 84,621 | 4 | 0 |
| CD-STEN vs CD-NINF | 123,877 | 4,883 | 261 |

A summary of the results found from the methylation (DMPs and DMRs) and gene expression (DEGs) analyses.

<https://doi.org/10.1371/journal.pone.0209656.t002>

10A (*WNT10A*) and Tenascin-X (*TNXB*) when comparing CD with non-CD and STEN with NINF, respectively (Fig 2A and 2B).

To understand the functional implication, we performed pathway enrichment analyses on hypo- and hypermethylated DMRs separately. As only few DMRs were found for the comparison INF vs NINF, we performed enrichment analyses only on the DMRs found when comparing CD with non-CD and STEN with NINF. The CD vs non-CD DMRs revealed enriched hypermethylation for ECM-processing, whereas tumor necrosis factor (TNF) receptor superfamily members were enriched for hypomethylation (Fig 2A and S3 Table). STEN vs NINF hypermethylated DMRs were enriched for various pathways associated to extracellular matrix and collagen biosynthesis, whereas hypomethylated DMRs were enriched for smooth muscle contraction, focal adhesion and various other signaling pathways (Fig 2B and S3 Table).

Downregulation of genes involved in extracellular matrix processes associated to stenosis

Following the methylation analyses, we sought to investigate what differences could be observed at the level of gene expression. Analysis of the gene expression profiles yielded fewer

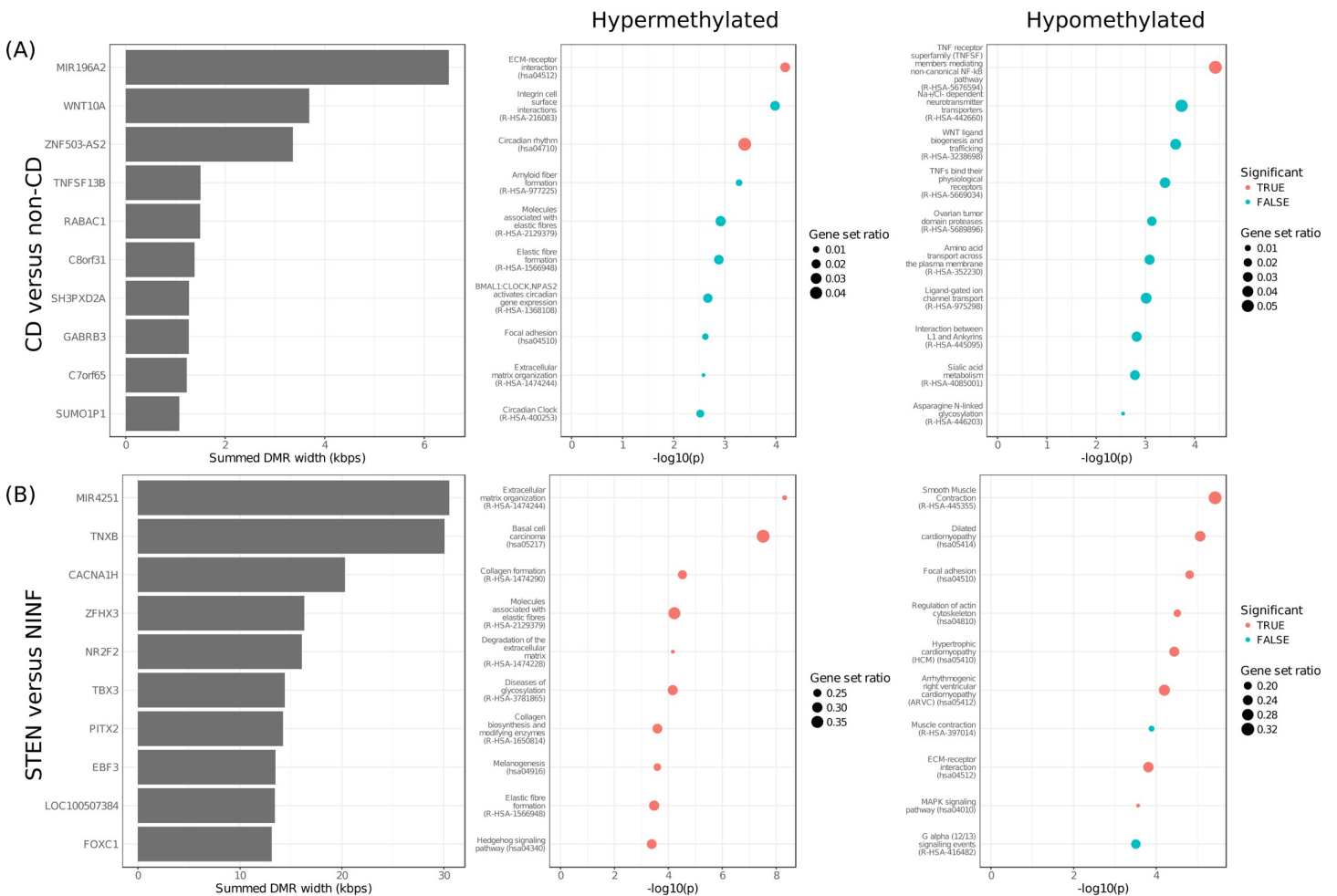


Fig 2. Enrichment analyses of the DMRs. Enrichment analyses results of the DMRs when comparing (A) CD with non-CD and (B) STEN with NINF. From left to right: Top 10 genes with the longest aggregated DMR, top 10 enriched pathways for the hypermethylated DMRs, and top 10 enriched pathways for the hypomethylated DMRs.

<https://doi.org/10.1371/journal.pone.0209656.g002>

results than the methylation analyses. Overall, we observed 11, 0 and 261 differentially expressed genes (DEGs) when comparing CD with non-CD, INF with NINF, and STEN with NINF, respectively (Tables 2 and S4). Like the methylation data, most DEGs were found when comparing STEN with NINF. Overall, we observed a general downregulation of the DEGs as visible from the volcano plot (S3 Fig).

Pathway analysis of the transcriptional changes when comparing CD with non-CD genes revealed upregulation of genes associated with RNA processing and downregulation of genes associated with translation (Fig 3A). Transcriptional changes when comparing STEN with NINF indicated upregulation of genes associated with RNA processing and downregulation of genes associated to elastic fiber formation, ECM proteoglycans, and extracellular matrix organization (Fig 3B and S5 Table).

Integrative methylation and expression analysis suggests concordant dysregulation of genes associated to PRKACA and E2F1

We subsequently integrated the DNA methylation and gene expression data by searching for genes that were differentially expressed and differentially methylated, and quantified the correlation through an expression quantitative trait methylation analysis (eQTM; S6 Table). No overlap was observed when comparing CD with non-CD or INF with NINF (Fig 4). When comparing STEN with NINF, we observed 76 DEGs that were associated to a DMR as well

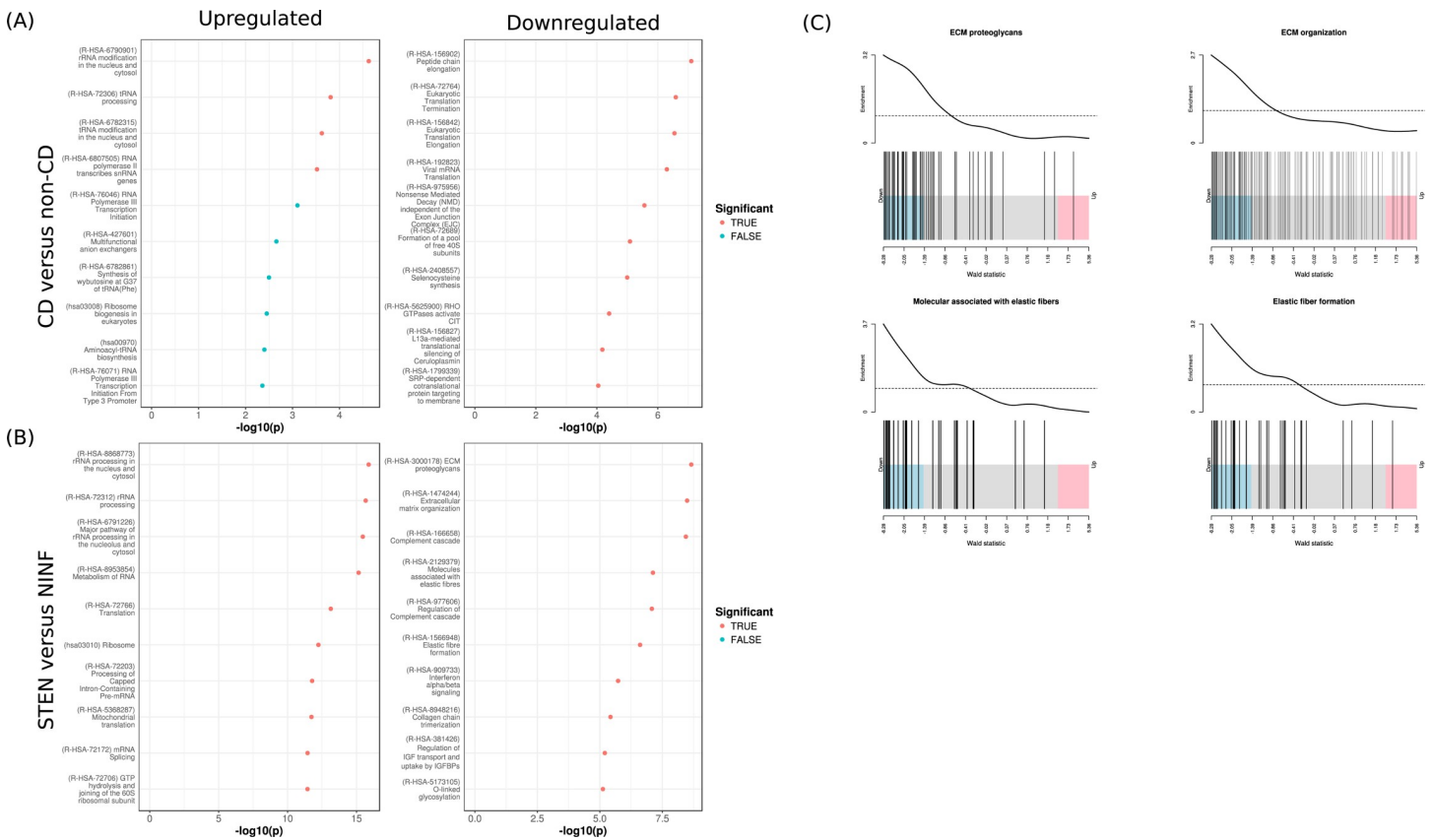


Fig 3. Enrichment analyses of the DEGs. Enrichment analyses results when comparing (A) CD with non-CD and (B) STEN with NINF. Top 10 enriched pathways for up- and downregulated genes on the left and right, respectively. (C) Barcode plots depicting the gene enrichment for ECM-associated pathways: “Molecules associated with elastic fibers”, “Elastic fiber formation”, “ECM proteoglycans”, and “Extracellular matrix organization”.

<https://doi.org/10.1371/journal.pone.0209656.g003>

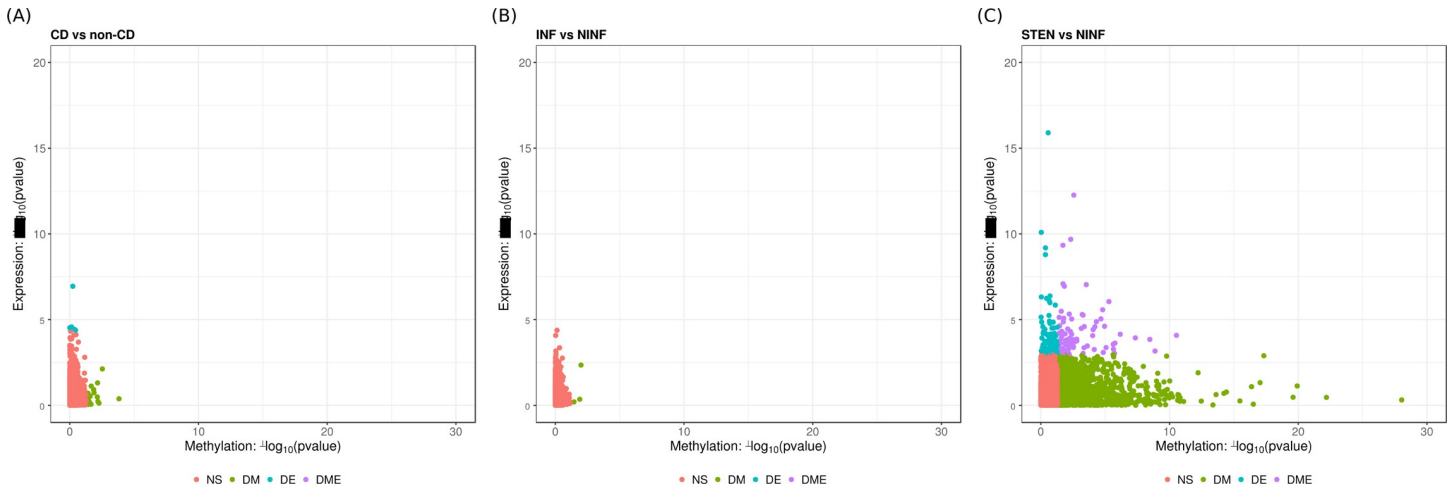


Fig 4. Methylation-expression integration. Overlap of $-\log_{10}(p\text{-value})$ of the results observed for the DMR analysis (x-axis) and the DE analysis (y-axis) for (A) CD vs non-CD, (B) INF vs NINF, and (C) STEN vs NINF. Colors represent statistical significance: red represents non-significant ('NS'), green represents differentially methylated ('DM'), blue represents differentially expressed ('DE'), and purple represents differentially methylated and expressed ('DME').

<https://doi.org/10.1371/journal.pone.0209656.g004>

(DMEGs). Overrepresentation analyses of the DMEGs corroborated our observations on the methylation and expression data alone with significant overrepresentation was for genes interacting with elastin, as well as genes encoding for proteins that are part of the transforming growth factor β (TGF β)-, and fibroblast growth factor receptor (FGF:FGFR) protein complexes (S7 Table).

To understand whether the DMEGs were interconnected, we performed an induced network analysis (Fig 5). Overall, two genes were observed that appeared to interact with most DMEGs, namely protein kinase CAMP-activated catalytic subunit alpha (*PRKACA*) and E2F transcription factor 1 (*E2F1*). Interestingly, *PRKACA* or *E2F1* were neither differentially methylated nor differentially expressed (Fig 6A). We therefore investigated whether the genes associated to *PRKACA* and *E2F1* were co-expressed. Pairwise correlation analyses suggested strong correlations for 9 genes, namely Wnt family member 2B (*WNT2B*), Serpin Family F Member 1 (*SERPINF1*), Myelin Basic Protein (*MBP*), Fibroblast Growth Factor Receptor 4 (*FGFR4*), apolipoprotein E (*APOE*), Activin A Receptor Like Type 1 (*ACVRL1*), Fibroblast Growth Factor Receptor 1 (*FGFR1*), Zinc Ring Finger Protein Like 1 (*ZFP36L1*), E2F transcription factor 7 (*E2F7*) (Figs 6B and S4). The strongest positive gene-gene correlations were observed primarily among *FGFR4*, *SERPINF1*, and *WNT2B*, whereas a strong inverse correlation was observed for *E2F7* (Table 3).

Discussion

In this study, we performed an integrative analysis of DNA methylation and gene expression to understand the intrinsic changes associated to CD-induced fibrosis. To this end, fibroblasts were obtained from ileal tissue at macroscopically-defined distinct stages of CD as well as from non-CD patients. As resection material represents a mixed cell population, we cultured the sample such that only fibroblasts would remain. We acknowledge that growing the samples in culture affects DNA methylation [52] and gene expression [53,54]. However, as all samples were passaged, we corrected for passage by including it as a covariate in the DNA methylation and gene expression analyses.

We observed most differences when comparing STEN with NINF fibroblasts. Conversely, few changes were observed when comparing CD with non-CD, or INF with NINF. We

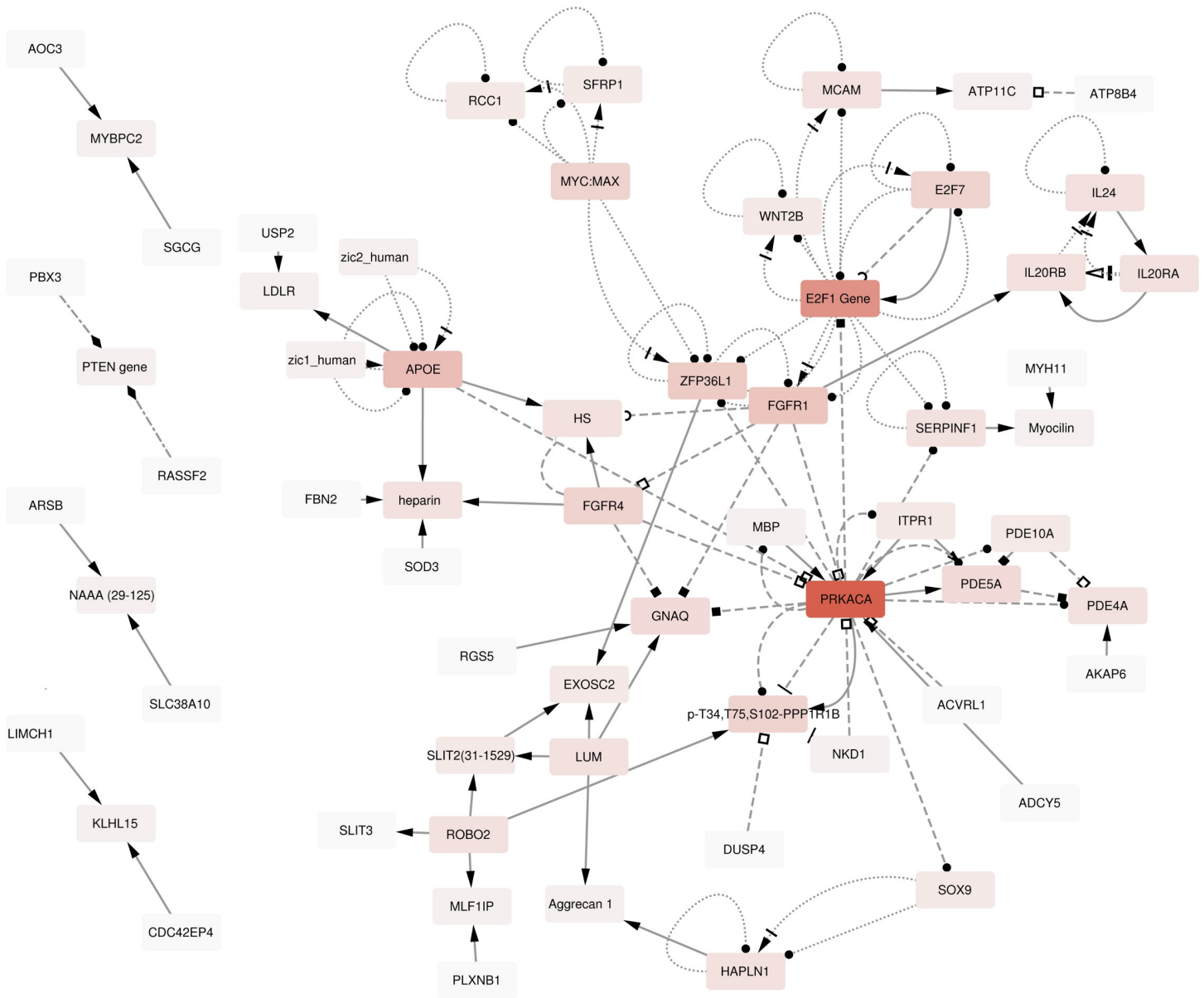


Fig 5. Induced network analysis. Induced network analysis of the DMEGs generated by the ConsensusPathDB. Edges represent the relationships between genes, which are represented as nodes. The intensity of the color of a node is proportional to the number of interactions known for that entity. Dashed lines represents biochemical interactions, dotted lines represents gene regulatory interactions, dashed-dotted lines represents genetic interactions and solid lines represent protein-protein interactions. Arrowheads represents the directionality of the interaction with solid squares representing activators, open squares representing enzymatic activity, diamonds representing genetic interactors, solid arrows representing physical interactors, solid circles representing products, the "T" representing repressors, the "C" representing substrates, the dashed solid arrow representing transcribed genes and the dashed open arrow representing transcription factors.

<https://doi.org/10.1371/journal.pone.0209656.g005>

hypothesize however that the limited sample size of the INF cohort precluded us from finding any meaningful results. By performing pathway analyses on the DMRs and DEGs we observed

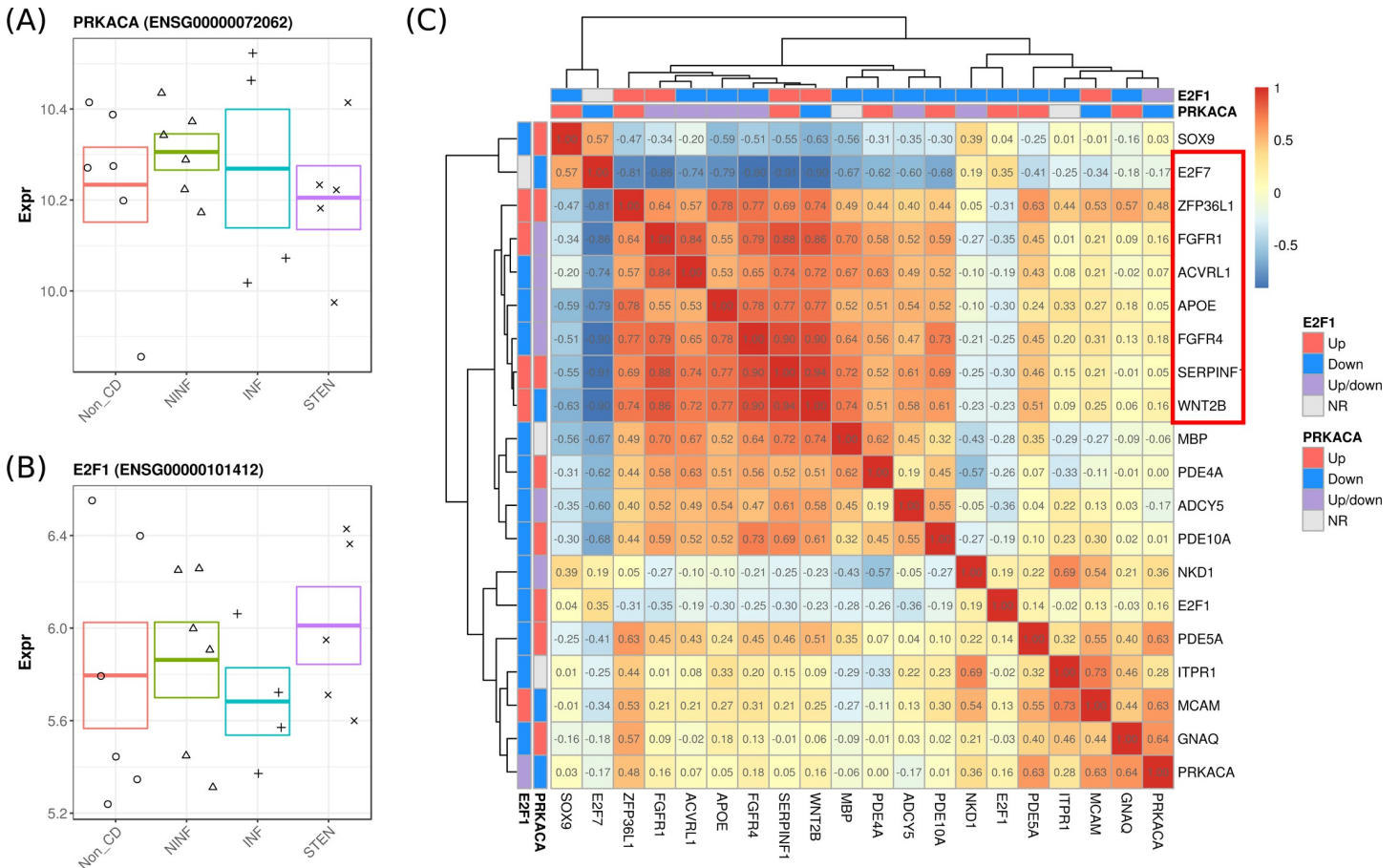


Fig 6. Overview of the PRKACA/E2F1-associated genes. Jitter plot representing the gene expression for the highly-interconnected genes (A) PRKACA and (B) E2F1. Error bars represent the standard error. (C) Heatmap representing the pairwise gene correlation coefficients for the genes linked to PRKACA and E2F1. Colored bars above the heatmap represent the relationship of the genes with PRKACA and E2F1, where upstream genes ('Up') are represented in red, downstream genes ('Down') in blue, up and downstream genes ('Up/down') in purple, and genes with no relationship ('NR') in grey. Highlighted in red are the genes whose absolute inter-gene correlations are higher than 0.7.

<https://doi.org/10.1371/journal.pone.0209656.g006>

Table 3. PRKACA/E2F1-associated DMEGs.

| Coordinates | nCpGs | Gene | Ensembl | Entrez | Correlation | p_correlation | p_DE | p_DM |
|--------------------------|-------|----------|-----------------|--------|----------------------|---------------|----------|----------|
| chr1:113054687–113056390 | 6 | WNT2B | ENSG00000134245 | 7482 | -0.88 [-0.97, -0.39] | 0.0583 | 0.000221 | 0.006753 |
| chr12:52299524–52301970 | 10 | ACVRL1 | ENSG00000139567 | 94 | -0.92 [-0.99, -0.63] | 0.0377 | 9.02E-06 | 2.15E-05 |
| chr12:77771462–77773503 | 5 | E2F7 | ENSG00000165891 | 144455 | -0.8 [-0.92, -0.29] | 0.0686 | 8.21E-08 | 0.018861 |
| chr14:69052728–69053361 | 3 | ZFP36L1 | ENSG00000185650 | 677 | -0.18 [-0.91, 0.65] | 0.7015 | 0.000153 | 0.009438 |
| chr17:1664329–1666607 | 10 | SERPINF1 | ENSG00000132386 | 5176 | -0.88 [-0.99, -0.43] | 0.0504 | 0.000236 | 1.75E-06 |
| chr18:74779597–74781719 | 4 | MBP | ENSG00000197971 | 4155 | -0.86 [-0.95, -0.4] | 0.0619 | 0.00042 | 0.002975 |
| chr19:45407860–45407945 | 3 | APOE | ENSG00000130203 | 348 | -0.78 [-0.96, -0.1] | 0.0473 | 0.00024 | 0.028636 |
| chr5:176515533–176516968 | 7 | FGFR4 | ENSG00000160867 | 2264 | -0.61 [-0.95, 0.35] | 0.2519 | 0.000268 | 0.00579 |
| chr8:38286241–38288404 | 6 | FGFR1 | ENSG00000077782 | 2260 | -0.85 [-0.96, -0.37] | 0.058 | 0.000102 | 0.024728 |

Columns represent the coordinates of the DMR, the associated gene name, the number of CpGs encompassed by the DMR, the Ensembl gene ID, the Entrez ID, the methylation-expression Pearson correlation coefficient with the 95% confidence intervals, the p-value of the correlation coefficient, the p-value of the DE analysis, and the p-value of the DMR analysis.

<https://doi.org/10.1371/journal.pone.0209656.t003>

concordant dysregulation for pathways associated to cellular differentiation, morphogenesis, and ECM remodeling. In particular, we observed consistent downregulation and promoter hypermethylation of genes associated with ECM processing and elastic fiber formation, implying systematic downregulation. Surprisingly, ECM-associated genes were found to be upregulated for idiopathic pulmonary- (IPF) [55,56], lung- [57], cardiac- [58], and CD-associated ileal fibrosis [59]. Despite observing similarly affected pathways, we are currently unsure why our results contrast previous findings.

As the methylation and gene expression analyses implicated similar pathways, we integrated the DMRs and the DEGs by overlapping the datasets and performing an eQTM analysis. Through induced network analysis, we identified two genes that interacted with most DMEGs, namely *PRKACA* and *E2F1*. *PRKACA* encodes one of the catalytic subunits of protein kinase A (PKA) and plays an important role in meiosis [60,61] and glucose metabolism [62]. Given its role in several pathways, dysregulation of PKA has been associated with multiple disorders including cardiovascular diseases [63], tumor formation [64], and fibrolamellar hepatocellular carcinoma [65]. Interestingly, no difference in *PRKACA* gene expression was observed across the different phenotypes. *E2F1* is a transcription factor belonging to the family of E2F transcription factors. Despite the lack of statistical significance, our data suggested an increase in the level of *E2F1* gene expression when comparing STEN with non-CD and NINF fibroblasts. Recent studies on cholestatic liver fibrosis observed an increase in the gene expression of *E2F1*, where it was found to act as a transcription factor alongside nuclear receptor small heterodimer partner (NR0B2; SHP) and co-repressor EP300 Interacting Inhibitor Of Differentiation 1 (EID1) in controlling the gene expression of Early Growth Response 1 (*EGR1*) [66], the latter of which has been implicated in the development of fibrosis [67–71].

Investigation of the DMEGs associated to *PRKACA/E2F1* revealed strong co-expression. Moreover, the methylation and the expression of the DMEGs were strongly correlated suggesting concordant dysregulation. Many of the *PRKACA/E2F1*-associated genes have been implicated in fibrotic processes previously. *SERPINF1* (S4B Fig), also known as pigment epithelium-derived factor (*PEDF*), was found to exhibit anti-angiogenic properties [72] by cleaving the vascular endothelial growth factor (VEGF) receptor 1 [73]. Our data indicated that *SERPINF1* expression was downregulated in stenotic fibroblasts. Conversely, *E2F7* (S4I Fig) was found to promote angiogenesis through transcriptional activation of *VEGFA* [74] and was upregulated in stenotic fibroblasts, which corroborates previous findings in mice where *E2F7* was found to be upregulated in renal fibrotic tissue [75]. Taken together, the observed downregulation of *SERPINF1* and upregulation of *E2F7* could promote angiogenesis, which is a characteristic of IBD [76,77] and fibrosis [78].

Just like *E2F1*, *E2F7* belongs to the family of E2F transcription factors, which play a central role in a wide range of biological processes such as differentiation, cell division [79], and DNA repair [80]. E2F transcription factors interact with several fibroblast growth factor receptors by regulating *FGFR1* (S4G Fig) [81] and *FGFR2* [82]. *FGFR1* suppresses TGF β and mitogen-activated protein kinase kinase kinase 4 (MAP4K4) [83], which is involved in endothelial-mesenchymal transition (EndoMT). Excessive EndoMT was found to contribute to cardiac [84–86] and idiopathic lung fibrosis [87]. Downregulation of *FGFR1* could therefore induce EndoMT, which could contribute towards the observed fibrotic phenotype [86]. Interestingly, the opposite effect was observed for *FGFR4* (S4D Fig), whose gene expression was downregulated in stenotic fibroblasts. In hepatocellular carcinoma samples, *FGFR4* expression was found to be increased alongside the expression of TGF β [88], suggesting that an increase in expression contributes towards fibrosis.

Besides the regulation of FGF pathways, E2F transcription factors also affect WNT pathways [89] primarily through *E2F1*, which was found to suppress Wnt/ β -catenin signaling

pathway by activating inhibitor of β -catenin and TCF4 (ICAT) [90]. Moreover, Wnt signaling was found to induce epithelial to mesenchymal transition, which, just like EndoMT, is a contributing factor of fibrosis [86]. Among the *PRKACA/E2F1* genes, we observed downregulation of Wnt signaling pathway member *WNT2B*, whose expression was correlated with an increase in methylation (S4A Fig). As IBD-associated mutations of constituent genes within the Wnt signaling pathway are rare, it was speculated that the epigenetic landscape surrounding Wnt-related genes were likely affected in CD [91]. Our data alongside others' [24,92] show that the expression of *WNT2B* is downregulated in STEN relative to NINF fibroblasts, which correlates with an increased methylation signal. STAT6-deficient mice, which display a delayed wound-healing phenotype akin to fibrosis, displayed diminished gene expression of *Wnt2b*, *Wnt7b*, and *Wnt10a* after 2,4,6-Trinitrobenzenesulfonic acid (TNBS) treatment [92]. Moreover, STAT6-deficient mice treated with TNBS displayed diminished accumulation of the classical WNT signaling protein β -catenin in the nucleus of mucosal cells relative to TNBS-treated control mice corroborating the impaired gene expression of *Wnt2b* [92].

Altogether, we observe that multiple components of the interconnected E2F, WNT, and FGF pathways [93] are dysregulated at the level of DNA methylation and gene expression. As the E2F, WNT and FGF pathways are important for cellular differentiation, proliferation, and migration, aberrant behavior thereof could underlie tissue remodeling processes, resulting in the observed fibro-stenotic phenotype [94–96].

Similar methylomic and transcriptomic changes were observed for genes encoding proteins that are involved in lipid metabolism. *APOE* was found to be downregulated, which was correlated with an increase in methylation (S4E Fig). *APOE*-deficient mice were found to develop metabolic syndromes, non-alcoholic steatohepatitis and liver fibrosis after being fed a cholesterol and fat rich diet or a methionine-choline-deficient-diet (MCD) [97]. Similarly, we observed *ZFP36L1* to be downregulated (S4H Fig), which regulates Cytochrome P450 Family 7 Subfamily A Member 1 (*CYP7A1*) mRNA [98]. *CYP7A1* is a rate limiting enzyme involved in cholesterol metabolism into bile acid [99]. Downregulation of *ZFP36L1* can therefore increase bile production leading to bile acid malabsorption, which is a common sign of IBD [100].

By performing integrated analyses of the methylome and the transcriptome we have observed changes in pathways associated to ECM processes and lipid metabolism. By narrowing our search to genes that were affected at the level of methylation and expression, we extracted novel targets for future studies. Nonetheless, further research is needed to validate the aforementioned results, where it would be important to investigate whether protein expression of the DMEGs corroborates the observed transcriptional and methylomic changes. Furthermore, additional research is necessary to understand the directionality of the methylation-expression relationship to ascertain causality. In particular, it would be worthwhile to investigate the effect and possibility of rectifying the aberrant methylation pattern, which would provide us with more insight into the intrinsic mechanisms underlying CD-associated fibrosis.

Supporting information

S1 Fig. Principal component analysis methylation and expression. Correlation of the degree and passage with each principal component for the (A) methylation data and (B) expression data. (PDF)

S2 Fig. Volcano plot of the CpG loci on the Illumina EPIC BeadChip array. The y-axis depicts the statistical significance ($-\log_{10}(p\text{-value})$) and x-axis depicts the percentage difference in methylation. (A) CD versus non-CD, (B) INF versus NINF, and (C) STEN vs NINF. Colors indicate whether a CpG is differentially methylated with a large effect size (Beta > 0.2; 'sig. interesting'), differentially methylated with a small effect size ('significant'), or not

differentially methylated ('non-significant'). The top 10 DMPs are labelled with their Illumina probe ID.

(PDF)

S3 Fig. Volcano plot of the genes measured through RNAseq experiment. The y-axis depicts the statistical significance ($-\log_{10}(\text{p-value})$) and the x-axis the \log_2 fold change. (A) CD versus non-CD, (B) INF versus NINF, and (C) STEN vs NINF. Colors indicate whether a gene is differentially expressed with a large effect size ($\log_{2}\text{FC} > 1$; 'sig. interesting'), differentially expressed with a small effect size ('significant'), or not differentially expressed ('non-significant'). The top 10 DMPs are labelled with their Ensembl gene ID.

(PDF)

S4 Fig. Summary plots of the DMEGs. (A) WNT2B, (B) SERPINF1, (C) MBP, (D) FGFR4, (E) APOE, (F) ACVRL1, (G) FGFR1, (H) ZFP36L1, and (I) E2F7. At the top: Genomic coordinates at the top represent the chromosome and the genomic positions of the DMRs with the gene of interest highlighted in red. Bottom left: Detailed genome plot of the methylation values of the CpGs that comprise the DMR of interest. Bottom middle: Plot of the expression representing the mean log-transformed expression and the standard error. Bottom right: Correlation plot of the log transformed expression on the x-axis against the mean methylation (Beta) of the DMR on the y-axis for the 9 samples present in both the methylation and expression experiment.

(PDF)

S1 Table. Overlapping samples. An overview of all the samples included in the methylation and expression studies. Details include the sample, patient, and passage number. Samples that were included in both the methylation and expression study are shown in bold text.

(XLSX)

S2 Table. Differentially methylated regions. Differentially methylated regions as found for CD vs non-CD (Tab 1), CD-inflamed vs CD-non-inflamed (Tab 2), and CD-stenotic vs CD-non-inflamed (Tab 3). Columns represent the coordinates of the DMR, the number of CpGs encompassed, the Stouffer statistic that represents a summary significance statistic of the DMR, the mean methylation signal across the DMR, the Ensembl gene ID, the gene symbol, and a gene name.

Tab 1: CD vs non-CD.

Tab 2: INF vs NINF.

Tab 3: STEN vs NINF.

(XLSX)

S3 Table. DMR pathway enrichment. Columns represent the database, the gene set ID, the description of the gene set, the enrichment p -value, the BH-adjusted p -value, the number of genes within the set, the number of observed genes from the set, the average gene length of the genes within the set, the Entrez IDs for the genes located in the gene set.

Tab 1: CD vs non-CD hypermethylated DMRs.

Tab 2: CD vs non-CD hypomethylated DMRs.

Tab 3: STEN vs NINF hypermethylated DMRs.

Tab 4: STEN vs NINF hypomethylated DMRs.

(XLSX)

S4 Table. Differentially expressed genes. Differentially expressed genes as found for the CD vs non-CD (Tab 1), CD-inflamed vs CD-non-inflamed (Tab 2), and CD-stenotic vs CD-non-inflamed (Tab 3). Columns represent the \log_2 fold change, the standard error of the \log_2 fold

change, the Wald statistic, the p -value, the BH-adjusted p -value, the gene symbol, the Entrez ID, and the Ensembl gene ID.

Tab 1: CD vs non-CD.

Tab 2: INF vs NINF.

Tab 3: STEN vs NINF.

(XLSX)

S5 Table. DEG gene set enrichment. Columns represent the database, the gene set ID, the description of the gene set, the enrichment p -value, the BH-adjusted p -value, the number of genes within the set, the number of observed genes from the set, the average gene length of the genes within the set, the Entrez IDs for the genes located in the gene set.

Tab 1: CD vs non-CD upregulated genes.

Tab 2: CD vs non-CD downregulated genes.

Tab 3: STEN vs NINF upregulated genes.

Tab 4: STEN vs NINF downregulated genes.

(XLSX)

S6 Table. DMEGs: Differentially methylated and expressed genes as found for STEN vs NINF. Columns represent the coordinates of the DMR, the associated gene name, the number of CpGs encompassed by the DMR, the Ensembl gene ID, the Entrez ID, the methylation-expression Pearson correlation coefficient alongside the 95% confidence intervals, the p -value of the correlation coefficient, the p -value of the DE analysis, and the p -value of the DMR analysis.

(XLSX)

S7 Table. DMEGs gene set overrepresentation analyses against all the genes measured as measured by CPDB.

Tab 1: Network neighborhood-based entity sets (NESTs). Columns represent the p -value, the BH-adjusted p -value, the name of the center, the Entrez ID of the NEST, the size of the NEST, the effective size of the NEST, the Ensembl gene IDs of the DMEGs within the NEST, and the sources of the NEST.

Tab 2: Pathway-based sets. Columns represent the p -value, the BH-adjusted p -value, the source database, the ID, the size of the gene set, the effective size of the gene set, and the Ensembl gene IDs of the DMEGs within the gene set.

(XLSX)

Acknowledgments

The authors wish to thank Dutton R. Hauhart (Reitz Ink) for making edits to this manuscript and the patients for participating in this study.

Author Contributions

Conceptualization: Manon E. Wildenberg, Peter Henneman, Anje A. te Velde.

Data curation: Andrew Y. F. Li Yim.

Formal analysis: Andrew Y. F. Li Yim.

Funding acquisition: Wouter J. de Jonge, Peter Henneman, Anje A. te Velde.

Investigation: Jessica R. de Bruyn, Nicolette W. Duijvis.

Project administration: Manon E. Wildenberg, Peter Henneman, Anje A. te Velde.

Resources: Wouter J. de Jonge, Christianne J. Buskens, Geert R. D’Haens, Peter Henneman, Anje A. te Velde.

Software: Andrew Y. F. Li Yim.

Supervision: Catriona Sharp, Enrico Ferrero, Wouter J. de Jonge, Manon E. Wildenberg, Marcel M. A. M. Mannens, Christianne J. Buskens, Geert R. D’Haens, Peter Henneman, Anje A. te Velde.

Visualization: Andrew Y. F. Li Yim.

Writing – original draft: Andrew Y. F. Li Yim, Jessica R. de Bruyn, Nicolette W. Duijvis.

Writing – review & editing: Catriona Sharp, Enrico Ferrero, Wouter J. de Jonge, Manon E. Wildenberg, Marcel M. A. M. Mannens, Christianne J. Buskens, Geert R. D’Haens, Peter Henneman, Anje A. te Velde.

References

1. Rieder F, de Bruyn JR, Pham BT, Katsanos K, Annese V, Higgins PDR, et al. Results of the 4th Scientific Workshop of the ECCO (Group II): Markers of intestinal fibrosis in inflammatory bowel disease. *J Crohn’s Colitis*. 2014; 8: 1166–1178. <https://doi.org/10.1016/j.crohns.2014.03.009> PMID: 24726695
2. Rieder F, Brenmoehl J, Leeb S, Scholmerich J, Rogler G. Wound healing and fibrosis in intestinal disease. *Gut*. 2007; 56: 130–139. <https://doi.org/10.1136/gut.2006.090456> PMID: 17172588
3. Burke JP, Mulsow JJ, O’Keane C, Docherty NG, Watson RWG, O’Connell PR. Fibrogenesis in Crohn’s disease. *Am J Gastroenterol*. 2007; 102: 439–448. <https://doi.org/10.1111/j.1572-0241.2006.01010.x> PMID: 17156147
4. Wynn T. Cellular and molecular mechanisms of fibrosis. *J Pathol*. 2008; 214: 199–210. <https://doi.org/10.1002/path.2277> PMID: 18161745
5. Johnson LA, Rodansky ES, Sauder KL, Horowitz JC, Mih JD, Tschumperlin DJ, et al. Matrix stiffness corresponding to strictured bowel induces a fibrogenic response in human colonic fibroblasts. *Inflamm Bowel Dis*. 2013; 19: 891–903. <https://doi.org/10.1097/MIB.0b013e3182813297> PMID: 23502354
6. Liu JZ, van Sommeren S, Huang H, Ng SC, Alberts R, Takahashi A, et al. Association analyses identify 38 susceptibility loci for inflammatory bowel disease and highlight shared genetic risk across populations. *Nat Genet*. 2015; 47. <https://doi.org/10.1038/ng.3359> PMID: 26192919
7. Manolio TA, Collins FS, Cox NJ, Goldstein DB, Hindorf LA, Hunter DJ, et al. Finding the missing heritability of complex diseases. *Nature*. Nature Publishing Group; 2009; 461: 747–753. <https://doi.org/10.1038/nature08494> PMID: 19812666
8. Jostins L, Ripke S, Weersma RK, Duerr RH, McGovern DP, Hui KY, et al. Host-microbe interactions have shaped the genetic architecture of inflammatory bowel disease. *Nature*. England, England: Nature Publishing Group; 2012; 491: 119–24. <https://doi.org/10.1038/nature11582> PMID: 23128233
9. Lee JC, Biasci D, Roberts R, Geary RB, Mansfield JC, Ahmad T, et al. Genome-wide association study identifies distinct genetic contributions to prognosis and susceptibility in Crohn’s disease. *Nat Genet*. Nature Publishing Group; 2017; 49: 262–268. <https://doi.org/10.1038/ng.3755> PMID: 28067912
10. Schultze JL. Macrophage tolerance in the gut: It is in the epigenome! *Eur J Immunol*. 2016; 46: 1838–1841. <https://doi.org/10.1002/eji.201646545> PMID: 27518699
11. Simon JM, Davis JP, Lee SE, Schaner MR, Gipson GR, Weiser M, et al. Alterations to chromatin in intestinal macrophages link IL-10 deficiency to inappropriate inflammatory responses. *Eur J Immunol*. 2016; 46: 1912–1925. <https://doi.org/10.1002/eji.201546237> PMID: 27159132
12. Stylianou E. Epigenetics: the fine-tuner in inflammatory bowel disease? *Curr Opin Gastroenterol*. United States; 2013; 29: 370–377. <https://doi.org/10.1097/MOG.0b013e328360bd12> PMID: 23743674
13. Jenke AC, Zilbauer M. Epigenetics in inflammatory bowel disease. *Curr Opin Gastroenterol*. 2012; 28: 577–584. <https://doi.org/10.1097/MOG.0b013e328357336b> PMID: 23041674
14. Polytaichou C, Koukos G, Iliopoulos D. Systems biology in inflammatory bowel diseases: ready for prime time. *Curr Opin Gastroenterol*. 2014; 30: 339–46. <https://doi.org/10.1097/MOG.000000000000081> PMID: 24837229

15. Berger SL, Kouzarides T, Shiekhattar R, Shilatifard A. An operational definition of epigenetics. *Genes Dev.* Nature Publishing Group, a division of Macmillan Publishers Limited. All Rights Reserved.; 2009; 23: 781–783. <https://doi.org/10.1101/gad.1787609> PMID: 19339683
16. O'Reilly S. Epigenetics in fibrosis. *Molecular Aspects of Medicine.* 2017. <https://doi.org/10.1016/j.mam.2016.10.001> PMID: 27720780
17. Li Yim AYW, Duijvis NW, Zhao J, de Jonge WJ, D'Haens GRAM, Mannens MMAM, et al. Peripheral blood methylation profiling of female Crohn's disease patients. *Clin Epigenetics.* Germany; 2016; 8: 65. <https://doi.org/10.1186/s13148-016-0230-5> PMID: 27279921
18. Karatzas PS, Gazouli M, Safioleas M, Mantzaris GJ. DNA methylation changes in inflammatory bowel disease. *Ann Gastroenterol Q Publ Hell Soc Gastroenterol.* Greece; 2014; 27: 125–132. Available: /pmc/articles/PMC3982627/?report=abstract
19. Nimmo ER, Prendergast JG, Aldhous MC, Kennedy NA, Henderson P, Drummond HE, et al. Genome-wide methylation profiling in Crohn's disease identifies altered epigenetic regulation of key host defense mechanisms including the Th17 pathway. *Inflamm Bowel Dis.* 2012; 18: 889–899. <https://doi.org/10.1002/ibd.21912> PMID: 22021194
20. McDermott E, Ryan EJ, Tosetto M, Gibson D, Burrage J, Keegan D, et al. DNA Methylation Profiling in Inflammatory Bowel Disease Provides New Insights into Disease Pathogenesis. *J Crohn's Colitis.* 2016; 10: 77–86. <https://doi.org/10.1093/ecco-jcc/jjv176> PMID: 26419460
21. Harris RA, Nagy-Szakal D, Mir SA, Frank E, Szigeti R, Kaplan JL, et al. DNA methylation-associated colonic mucosal immune and defense responses in treatment-naïve pediatric ulcerative colitis. *Epigenetics.* 2014; 9: 1131–1137. <https://doi.org/10.4161/epi.29446> PMID: 24937444
22. Yu W, Lin Z, Hegarty JP, Chen X, Kelly AA, Wang Y, et al. Genes Differentially Regulated by NKX2-3 in B Cells Between Ulcerative Colitis and Crohn's Disease Patients and Possible Involvement of EGR1. *Inflammation.* United States; 2012; 35: 889–899. <https://doi.org/10.1007/s10753-011-9390-9> PMID: 21968973
23. Cooke J, Zhang H, Greger L, Silva A-L, Massey D, Dawson C, et al. Mucosal genome-wide methylation changes in inflammatory bowel disease. *Inflamm Bowel Dis.* United States; 2012; 18: 2128–2137. <https://doi.org/10.1002/ibd.22942> PMID: 22419656
24. Sadler T, Bhasin JM, Xu Y, Barnholz-Sloan J, Chen Y, Ting AH, et al. Genome-wide analysis of DNA methylation and gene expression defines molecular characteristics of Crohn's disease-associated fibrosis. *Clin Epigenetics.* Clinical Epigenetics; 2016; 8: 30. <https://doi.org/10.1186/s13148-016-0193-6> PMID: 26973718
25. Chang C-W, Wong J-M, Tung C-C, Shih I-L, Wang H-Y, Wei S-C. Intestinal Stricture in Crohn's Disease. *Intest Res.* 2015; 13: 19. <https://doi.org/10.5217/ir.2015.13.1.19> PMID: 25691840
26. Kerami Z, Duijvis NW, Vogels EW, van Dooren FH, Moerland PD, te Velde AA. Effect of interleukin-17 on gene expression profile of fibroblasts from Crohn's disease patients. *J Crohn's Colitis.* 2014; 8: 1208–1216. <https://doi.org/10.1016/j.crohns.2014.02.009> PMID: 24637010
27. Satsangi J, Silverberg MS, Vermeire S, Colombel J-F. The Montreal classification of inflammatory bowel disease: controversies, consensus, and implications. *Gut.* England; 2006; 55: 749–753. <https://doi.org/10.1136/gut.2005.082909> PMID: 16698746
28. Leeb SN, Vogl D, Gunckel M, Kiessling S, Falk W, Goñke M, et al. Reduced Migration of Fibroblasts in Inflammatory Bowel Disease: Role of Inflammatory Mediators and Focal Adhesion Kinase. 2003; [https://doi.org/10.1053/S0016-5085\(03\)01348-9](https://doi.org/10.1053/S0016-5085(03)01348-9)
29. Ihaka R, Gentleman R. R: A Language for Data Analysis and Graphics. *J Comput Graph Stat.* [American Statistical Association, Taylor & Francis, Ltd., Institute of Mathematical Statistics, Interface Foundation of America]; 1996; 5: 299–314. <https://doi.org/10.2307/1390807>
30. Aryee MJ, Jaffe AE, Corrada-Bravo H, Ladd-Acosta C, Feinberg AP, Hansen KD, et al. Minfi: A flexible and comprehensive Bioconductor package for the analysis of Infinium DNA methylation microarrays. *Bioinformatics.* 2014; 30: 1363–1369. <https://doi.org/10.1093/bioinformatics/btu049> PMID: 24478339
31. van Iterson M, Tobi EW, Sliker RC, den Hollander W, Luijk R, Slagboom PE, et al. MethylAid: visual and interactive quality control of large Illumina 450k datasets. *Bioinformatics.* 2014; 30: 3435–3437. <https://doi.org/10.1093/bioinformatics/btu566> PMID: 25147358
32. Fortin J-PP, Labbe A, Lemire M, Zanke BW, Hudson TJ, Fertig EJ, et al. Functional normalization of 450k methylation array data improves replication in large cancer studies. *Genome Biol.* England; 2014; 15: 503. <https://doi.org/10.1186/s13059-014-0503-2> PMID: 25599564
33. Ritchie ME, Phipson B, Wu D, Hu Y, Law CW, Shi W, et al. limma powers differential expression analyses for RNA-sequencing and microarray studies. *Nucleic Acids Res.* 2015; 43: e47–e47. <https://doi.org/10.1093/nar/gkv007> PMID: 25605792

34. Smyth GK. Linear Models and Empirical Bayes Methods for Assessing Differential Expression in Microarray Experiments. *Stat Appl Genet Mol Biol*. 2004; 3: 1–25. <https://doi.org/10.2202/1544-6115.1027> PMID: 16646809
35. Peters TJ, Buckley MJ, Statham AL, Pidsley R, Samaras K, V Lord R, et al. De novo identification of differentially methylated regions in the human genome. *Epigenetics Chromatin*. 2015; 8: 6. <https://doi.org/10.1186/1756-8935-8-6> PMID: 25972926
36. Yu G, Wang LG, He QY. ChIP seeker: An R/Bioconductor package for ChIP peak annotation, comparison and visualization. *Bioinformatics*. 2015; 31: 2382–2383. <https://doi.org/10.1093/bioinformatics/btv145> PMID: 25765347
37. Zhou W, Laird PW, Shen H. Comprehensive characterization, annotation and innovative use of Infinium DNA methylation BeadChip probes. *Nucleic Acids Res*. 2016; gkw967. <https://doi.org/10.1093/nar/gkw967> PMID: 27924034
38. Du P, Zhang X, Huang C-C, Jafari N, Kibbe WA, Hou L, et al. Comparison of Beta-value and M-value methods for quantifying methylation levels by microarray analysis. *BMC Bioinformatics*. BioMed Central Ltd; 2010; 11: 587. <https://doi.org/10.1186/1471-2105-11-587> PMID: 21118553
39. Wickham H. *ggplot2: Elegant Graphics for Data Analysis* [Internet]. New York, NY: Springer-Verlag New York; 2009. Available: <http://ggplot2.org>
40. Horvath S, Gurven M, Levine ME, Trumble BC, Kaplan H, Allayee H, et al. An epigenetic clock analysis of race/ethnicity, sex, and coronary heart disease. *Genome Biol. Genome Biology*; 2016; 17: 171. <https://doi.org/10.1186/s13059-016-1030-0> PMID: 27511193
41. Andrews S. FastQC: a quality control tool for high throughput sequence data [Internet]. Available: <http://www.bioinformatics.babraham.ac.uk/projects/fastqc>
42. Dobin A, Davis CA, Schlesinger F, Drenkow J, Zaleski C, Jha S, et al. STAR: Ultrafast universal RNA-seq aligner. *Bioinformatics*. 2013; 29: 15–21. <https://doi.org/10.1093/bioinformatics/bts635> PMID: 23104886
43. Li H, Handsaker B, Wysoker A, Fennell T, Ruan J, Homer N, et al. The Sequence Alignment/Map format and SAMtools. *Bioinformatics*. 2009; 25: 2078–2079. <https://doi.org/10.1093/bioinformatics/btp352> PMID: 19505943
44. Liao Y, Smyth GK, Shi W. The Subread aligner: fast, accurate and scalable read mapping by seed-and-vote. *Nucleic Acids Res. England*; 2013; 41: e108. <https://doi.org/10.1093/nar/gkt214> PMID: 23558742
45. Love MI, Anders S, Huber W. Differential analysis of count data—the DESeq2 package [Internet]. *Genome Biology*. 2014. doi:10.1186/s13059-014-0550-8
46. Hahne F, Ivanek R. Visualizing Genomic Data Using Gviz and Bioconductor. In: Mathé E, Davis S, editors. *Statistical Genomics: Methods and Protocols*. New York, NY: Springer New York; 2016. pp. 335–351. https://doi.org/10.1007/978-1-4939-3578-9_16
47. Oda K, Yatera K, Izumi H, Ishimoto H, Yamada S, Nakao H, et al. Profibrotic role of WNT10A via TGF- β signaling in idiopathic pulmonary fibrosis. *Respir Res. Respiratory Research*; 2016; 17: 1–14. <https://doi.org/10.1186/s12931-015-0319-y>
48. Wu D, Smyth GK. Camera: A competitive gene set test accounting for inter-gene correlation. *Nucleic Acids Res*. 2012; 40: 1–12. <https://doi.org/10.1093/nar/gkr648>
49. Fabregat A, Sidiropoulos K, Garapati P, Gillespie M, Hausmann K, Haw R, et al. The reactome pathway knowledgebase. *Nucleic Acids Res. Oxford University Press*; 2018; 44: D481–D487. <https://doi.org/10.1093/nar/gkv1351> PMID: 26656494
50. Kanehisa M, Sato Y, Kawashima M, Furumichi M, Tanabe M. KEGG as a reference resource for gene and protein annotation. *Nucleic Acids Res*. 2016; 44: D457–D462. <https://doi.org/10.1093/nar/gkv1070> PMID: 26476454
51. Kamburov A, Wierling C, Lehrach H, Herwig R. ConsensusPathDB—A database for integrating human functional interaction networks. *Nucleic Acids Res*. 2009; 37: 623–628. <https://doi.org/10.1093/nar/gkn698> PMID: 18940869
52. Horvath S. DNA methylation age of human tissues and cell types. *Genome Biol*. 2013; 14: R115. <https://doi.org/10.1186/gb-2013-14-10-r115> PMID: 24138928
53. Neumann E, Riepl B, Knedla A, Lefèvre S, Tarner IH, Grifka J, et al. Cell culture and passaging alters gene expression pattern and proliferation rate in rheumatoid arthritis synovial fibroblasts. *Arthritis Res Ther*. 2010; 12: R83. <https://doi.org/10.1186/ar3010> PMID: 20462438
54. Januszzyk M, Rennert R, Sorkin M, Maan Z, Wong L, Whittam A, et al. Evaluating the Effect of Cell Culture on Gene Expression in Primary Tissue Samples Using Microfluidic-Based Single Cell Transcriptional Analysis. *Microarrays*. 2015; 4: 540–550. <https://doi.org/10.3390/microarrays4040540> PMID: 27600239

55. Selman M, Pardo A, Barrera L, Estrada A, Watson SR, Wilson K, et al. Gene expression profiles distinguish idiopathic pulmonary fibrosis from hypersensitivity pneumonitis. *Am J Respir Crit Care Med*. 2006; <https://doi.org/10.1164/rccm.200504-644OC> PMID: 16166619
56. Parker MW, Rossi D, Peterson M, Smith K, Sikstrom K, White ES, et al. Fibrotic extracellular matrix activates a profibrotic positive feedback loop. *J Clin Invest*. 2014; 124: 1622–1635. <https://doi.org/10.1172/JCI71386> PMID: 24590289
57. Blaauboer ME, Boeijen FR, Emson CL, Turner SM, Zandieh-Doulabi B, Hanemaaijer R, et al. Extracellular matrix proteins: A positive feedback loop in lung fibrosis? *Matrix Biol*. 2014; <https://doi.org/10.1016/j.matbio.2013.11.002> PMID: 24291458
58. Fan D, Takawale A, Lee J, Kassiri Z. Cardiac fibroblasts, fibrosis and extracellular matrix remodeling in heart disease. *Fibrogenesis Tissue Repair*. 2012; <https://doi.org/10.1186/1755-1536-5-15> PMID: 22943504
59. de Bruyn JR, van den Brink GR, Steenkamer J, Buskens CJ, Bemelman WA, Meisner S, et al. Fibrotenotic phenotype of myofibroblasts in crohn's disease is dependent on tissue stiffness and reversed by LOX inhibition. *J Crohn's Colitis*. 2018; 12: 849–859. <https://doi.org/10.1093/ecco-jcc/jjy036> PMID: 29672662
60. Duncan FE, Moss SB, Williams CJ. Knockdown of the cAMP-dependent protein kinase (PKA) Type I α regulatory subunit in mouse oocytes disrupts meiotic arrest and results in meiotic spindle defects. *Dev Dyn*. 2006; 235: 2961–2968. <https://doi.org/10.1002/dvdy.20930> PMID: 16937372
61. Kovo M, Kandli-Cohen M, Ben-Haim M, Galiani D, Carr DW, Dekel N. An active protein kinase A (PKA) is involved in meiotic arrest of rat growing oocytes. *Reproduction*. 2006; 132: 33–43. <https://doi.org/10.1530/rep.1.00824> PMID: 16816331
62. Lester LB, Faux MC, Nauert JB, Scott JD. Targeted protein kinase A and PP-2B regulate insulin secretion through reversible phosphorylation. *Endocrinology*. 2001; 142: 1218–1227. <https://doi.org/10.1210/endo.142.3.8023> PMID: 11181538
63. Bers DM. Calcium cycling and signaling in cardiac myocytes. *Annu Rev Physiol*. United States; 2008; 70: 23–49. <https://doi.org/10.1146/annurev.physiol.70.113006.100455> PMID: 17988210
64. Berthon AS, Szarek E, Stratakis CA. PRKACA: the catalytic subunit of protein kinase A and adrenocortical tumors. *Front Cell Dev Biol*. 2015; 3: 1–6. <https://doi.org/10.3389/fcell.2015.00001>
65. Kasthuber ER, Lalazar G, Houlihan SL, Tschaharganeh DF, Baslan T, Chen C-C, et al. DNAJB1–PRKACA fusion kinase interacts with β -catenin and the liver regenerative response to drive fibrolamellar hepatocellular carcinoma. *Proc Natl Acad Sci*. 2017; 201716483. <https://doi.org/10.1073/pnas.1716483114> PMID: 29162699
66. Zhang Y, Xu N, Xu J, Kong B, Copple B, Guo GL, et al. E2F1 is a novel fibrogenic gene that regulates cholestatic liver fibrosis through the Egr-1/SHP/EID1 network. *Hepatology*. 2014; 60: 919–930. <https://doi.org/10.1002/hep.27121> PMID: 24619556
67. Wu M, Melichian DS, de la Garza M, Gruner K, Bhattacharyya S, Barr L, et al. Essential Roles for Early Growth Response Transcription Factor Egr-1 in Tissue Fibrosis and Wound Healing. *The American Journal of Pathology*. 2009. pp. 1041–1055. <https://doi.org/10.2353/ajpath.2009.090241> PMID: 19679873
68. Yao J, Mackman N, Edgington TS, Fan ST. Lipopolysaccharide induction of the tumor necrosis factor- α promoter in human monocytic cells. Regulation by Egr-1, c-Jun, and NF- κ B transcription factors. *J Biol Chem*. United States; 1997; 272: 17795–17801. PMID: 9211933
69. Liu C, Adamson E, Mercola D. Transcription factor EGR-1 suppresses the growth and transformation of human HT-1080 fibrosarcoma cells by induction of transforming growth factor beta 1. *Proceedings of the National Academy of Sciences of the United States of America*. 1996. pp. 11831–11836. PMID: 8876223
70. Mundschauf LJ, Forman LW, Weng H, Faller DV. Platelet-derived growth factor (PDGF) induction of egr-1 is independent of PDGF receptor autophosphorylation on tyrosine. *J Biol Chem*. United States; 1994; 269: 16137–16142. PMID: 8206913
71. Jimenez SK, Sheikh F, Jin Y, Detillieux KA, Dhaliwal J, Kardami E, et al. Transcriptional regulation of FGF-2 gene expression in cardiac myocytes. *Cardiovasc Res*. 2004; 62: 548–557. <https://doi.org/10.1016/j.cardiores.2004.01.032> PMID: 15158147
72. Dawson DW, Volpert O V, Gillis P, Crawford SE, Xu H, Benedict W, et al. Pigment epithelium-derived factor: a potent inhibitor of angiogenesis. *Science*. United States; 1999; 285: 245–248. PMID: 10398599
73. Cai J, Jiang WG, Grant MB, Boulton M. Pigment epithelium-derived factor inhibits angiogenesis via regulated intracellular proteolysis of vascular endothelial growth factor receptor 1. *J Biol Chem*. 2006; 281: 3604–3613. <https://doi.org/10.1074/jbc.M507401200> PMID: 16339148

74. Weijts BGMW, Bakker WJ, Cornelissen PWA, Liang K-H, Schaftenaar FH, Westendorp B, et al. E2F7 and E2F8 promote angiogenesis through transcriptional activation of VEGFA in cooperation with HIF1. *EMBO J. Nature Publishing Group*; 2012; 31: 3871–3884. <https://doi.org/10.1038/emboj.2012.231> PMID: 22903062
75. Arvaniti E, Moulos P, Vakrakou A, Chatziantoniou C, Chadjichristos C, Kavvadas P, et al. Whole-transcriptome analysis of UUO mouse model of renal fibrosis reveals new molecular players in kidney diseases. *Sci Rep. Nature Publishing Group*; 2016; 6: 26235. <https://doi.org/10.1038/srep26235> PMID: 27189340
76. Karhausen J, Furuta GT, Tomaszewski JE, Johnson RS, Colgan SP, Haase VH. Epithelial hypoxia-inducible factor-1 is protective in murine experimental colitis. *J Clin Invest.* 2004; 114: 1098–1106. <https://doi.org/10.1172/JCI21086> PMID: 15489957
77. Carmeliet P, Jain RK. Molecular mechanisms and clinical applications of angiogenesis. *Nature.* 2011; 473: 298–307. <https://doi.org/10.1038/nature10144> PMID: 21593862
78. Elpek GÖ. Angiogenesis and liver fibrosis. *World J Hepatol.* 2015; 7: 377. <https://doi.org/10.4254/wjh.v7.i3.377> PMID: 25848465
79. Delgado I, Fresnedo O, Iglesias A, Rueda Y, Syn W-K, Zubiaga AM, et al. A role for transcription factor E2F2 in hepatocyte proliferation and timely liver regeneration. *Am J Physiol Gastrointest Liver Physiol.* 2011; 301: 20–31. <https://doi.org/10.1152/ajpgi.00481.2010.-E2F>
80. Chaussepied M, Ginsberg D, Weizmann U. E2F and signal transduction pathways. *Cell Cycle.* 2005; 4: 392–396. <https://doi.org/10.4161/cc.4.3.1556> PMID: 15701966
81. Kanai M, Tashiro E, Maruki H, Minato Y, Imoto M. Transcriptional regulation of human fibroblast growth factor receptor 1 by E2F-1. *Gene. Netherlands*; 2009; 438: 49–56. <https://doi.org/10.1016/j.gene.2009.03.004> PMID: 19303924
82. Tashiro E, Minato Y, Maruki H, Asagiri M, Imoto M. Regulation of FGF receptor-2 expression by transcription factor E2F-1. *Oncogene.* 2003; <https://doi.org/10.1038/sj.onc.1206636> PMID: 12944911
83. Li J, Shi S, Srivastava SP, Kitada M, Nagai T, Nitta K, et al. FGFR1 is critical for the anti-endothelial mesenchymal transition effect of N-Acetyl-seryl-Aspartyl-lysyl-proline via induction of the MAP4K4 pathway. *Cell Death Dis. Nature Publishing Group*; 2017; 8: 1–10. <https://doi.org/10.1038/s41419-017-0042-3>
84. Frid MG, Kale VA, Stenmark KR. Mature vascular endothelium can give rise to smooth muscle cells via endothelial-mesenchymal transdifferentiation: In vitro analysis. *Circ Res.* 2002; 90: 1189–1196. <https://doi.org/10.1161/01.RES.0000021432.70309.28> PMID: 12065322
85. Zeisberg EM, Tarnavski O, Zeisberg M, Dorfman AL, McMullen JR, Gustafsson E, et al. Endothelial-to-mesenchymal transition contributes to cardiac fibrosis. *Nat Med. United States*; 2007; 13: 952–961. <https://doi.org/10.1038/nm1613> PMID: 17660828
86. Rieder F, Fiocchi C. Mechanisms of tissue remodeling in inflammatory bowel disease. *Dig Dis.* 2013; <https://doi.org/10.1159/000353364> PMID: 24030223
87. Shimbori C, Bellaye PS, Xia J, Gauldie J, Ask K, Ramos C, et al. Fibroblast growth factor-1 attenuates TGF-β1-induced lung fibrosis. *J Pathol.* 2016; 240: 197–210. <https://doi.org/10.1002/path.4768> PMID: 27425145
88. Chen Z, Xie B, Zhu Q, Xia Q, Jiang S, Cao R, et al. FGFR4 and TGF-β1 expression in hepatocellular carcinoma: Correlation with clinicopathological features and prognosis. *Int J Med Sci.* 2013; 10: 1868–1875. <https://doi.org/10.7150/ijms.6868> PMID: 24324363
89. Hughes TA, Brady HJM. Cross-talk between pRb/E2F and Wnt/β-catenin pathways: E2F1 induces axin2 leading to repression of Wnt signalling and to increased cell death. *Exp Cell Res.* 2005; 303: 32–46. <https://doi.org/10.1016/j.yexcr.2004.09.014> PMID: 15572025
90. Wu Z, Zheng S, Li Z, Tan J, Yu Q. E2F1 suppresses Wnt/beta-catenin activity through transactivation of beta-catenin interacting protein ICAT. *Oncogene. England*; 2011; 30: 3979–3984. <https://doi.org/10.1038/onc.2011.129> PMID: 21532622
91. Dhir M, Montgomery EA, Glöckner SC, Schuebel KE, Hooker CM, Herman JG, et al. Epigenetic Regulation of WNT Signaling Pathway Genes in Inflammatory Bowel Disease (IBD) Associated Neoplasia. *J Gastrointest Surg.* 2008; 12: 1745–1753. <https://doi.org/10.1007/s11605-008-0633-5> PMID: 18716850
92. Cosín-Roger J, Ortiz-Masiá D, Calatayud S, Hernández C, Esplugues JV., Barrachina MD. The activation of Wnt signaling by a STAT6-dependent macrophage phenotype promotes mucosal repair in murine IBD. *Mucosal Immunol.* 2016; 9: 986–998. <https://doi.org/10.1038/mi.2015.123> PMID: 26601901

93. Yeo HC, Beh TT, Quek JLL, Koh G, Chan KKK, Lee DY. Integrated transcriptome and binding sites analysis implicates E2F in the regulation of self-renewal in human pluripotent stem cells. *PLoS One*. 2011; 6. <https://doi.org/10.1371/journal.pone.0027231> PMID: 22076139
94. Yu W, Lin Z, Pastor DM, Hegarty JP, Chen X, Kelly AA, et al. Genes regulated by Nkx2-3 in sporadic and inflammatory bowel disease-associated colorectal cancer cell lines. *Dig Dis Sci*. 2010; 55: 3171–3180. <https://doi.org/10.1007/s10620-010-1138-0> PMID: 20165982
95. Ornitz DM, Itoh N. The Fibroblast Growth Factor signaling pathway. *Wiley Interdisciplinary Reviews. Developmental Biology*. Hoboken, USA; 2015. pp. 215–266. <https://doi.org/10.1002/wdev.176> PMID: 25772309
96. Swiss VA, Casaccia P. Cell-Context Specific Role of the E2F/Rb Pathway in Development and Disease. *Glia*. 2010. pp. 377–390. <https://doi.org/10.1002/glia.20933> PMID: 19795505
97. Schierwagen R, Maybüchen L, Zimmer S, Hittatiya K, Bäck C, Klein S, et al. Seven weeks of Western diet in apolipoprotein-E-deficient mice induce metabolic syndrome and non-alcoholic steatohepatitis with liver fibrosis. *Sci Rep. Nature Publishing Group*; 2015; 5: 1–14. <https://doi.org/10.1038/srep12931> PMID: 26263022
98. Tarling EJ, Clifford BL, Cheng J, Morand P, Cheng A, Lester E, et al. RNA-binding protein ZFP36L1 maintains posttranscriptional regulation of bile acid metabolism. *J Clin Invest*. 2017; 127: 3741–3754. <https://doi.org/10.1172/JCI94029> PMID: 28891815
99. Chiang JYL. Bile acid metabolism and signaling in liver disease and therapy. *Liver Res. Elsevier Ltd*; 2017; 1: 3–9. <https://doi.org/10.1016/j.livres.2017.05.001> PMID: 29104811
100. Vitek L. Bile acid malabsorption in inflammatory bowel disease. *Inflamm Bowel Dis. United States*; 2015; 21: 476–483. <https://doi.org/10.1097/MIB.000000000000193> PMID: 25248001